The Histone Demethylase KDM6B Governs the Lyve1^{+} Perivascular Macrophage Phenotype to Control Adipose Tissue Expandability through BMP2 Signaling

Aznar Bastien et al.

Supplementary Figures and Tables

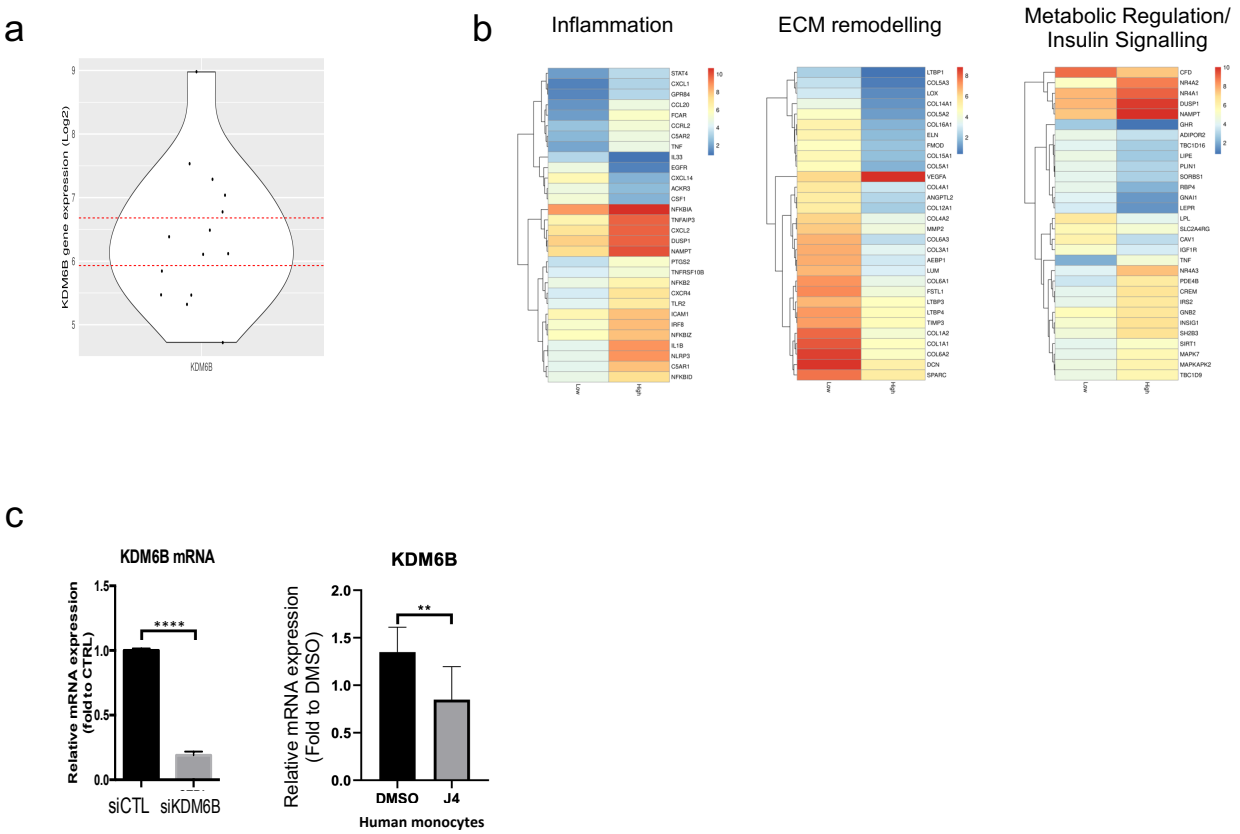

Supplementary Fig. 1 High KDM6B expression identifies anti-inflammatory CD14⁺ macrophages in human visceral adipose tissue

a, Violin plot of KDM6B mRNA in CD14⁺ macrophages isolated from visWAT of obese donors (n = 14). b, Bulk RNA-seq heat map of genes related to inflammation, extracellular-matrix remodelling and metabolic/insulin signalling in cells with high (n = 7) versus low (n = 7) KDM6B. c, Left, KDM6B mRNA after siRNA knock-down (siKDM6B) in CD14⁺ macrophages; right, KDM6B mRNA after treatment with the selective inhibitor GSK-J4 or inactive analogue GSK-J5 (each n = 4 donors). Data are mean ± s.e.m. Statistics: two-sided unpaired t-test (c) or DESeq2 Wald test with Benjamini–Hochberg correction (b). **P < 0.01; ****P < 0.0001.

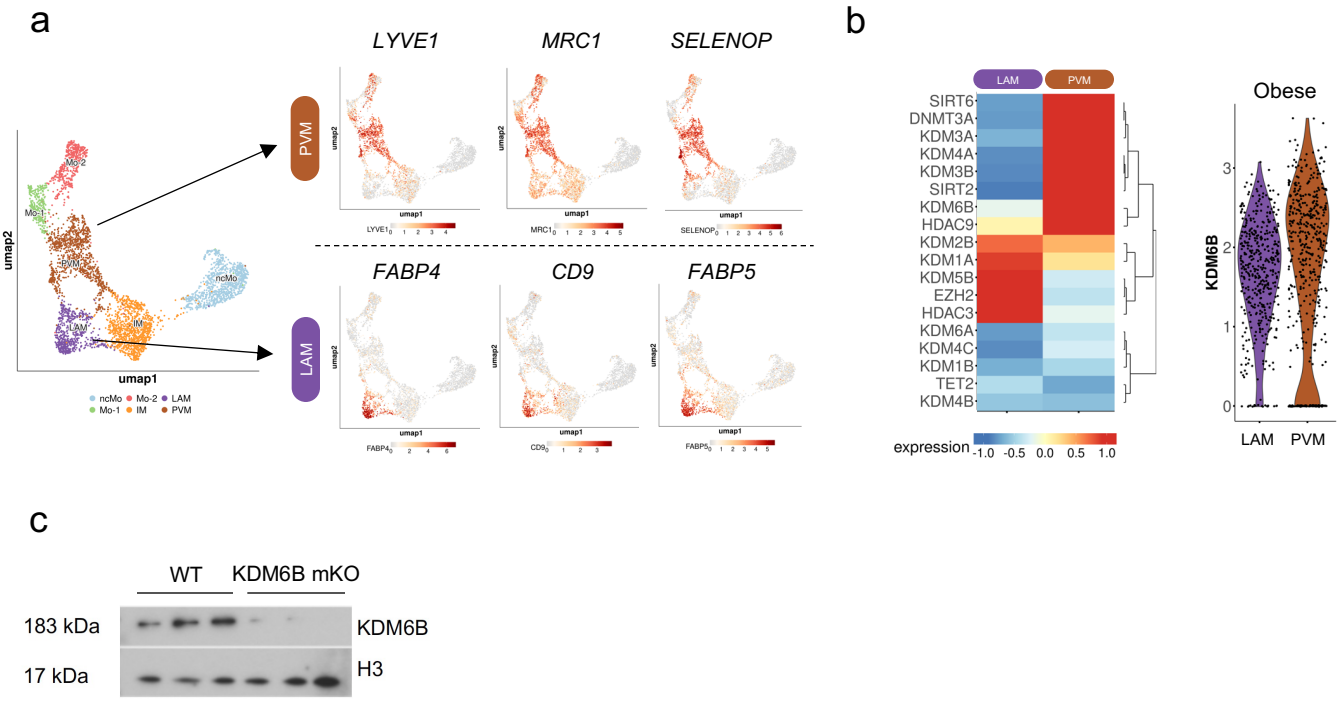

Supplementary Fig. 2 | KDM6B is enriched in perivascular macrophages

a, UMAP of single-cell RNA-seq from human visWAT highlighting PVM (LYVE1^{+}CD206^{+}) and LAM (TREM2^{+}) clusters and their marker genes (n = 4 donors). b, Heat map of JmjC-domain histone demethylases in PVMs versus LAMs. c, Immunoblot for KDM6B in bone-marrow-derived macrophages (BMDMs) from wild-type (WT) and myeloid Kdm6b-knockout (mKO) mice fed chow diet (n = 3 per genotype). Data are mean ± s.e.m. Statistics: Seurat Wilcoxon rank-sum test (a,b).

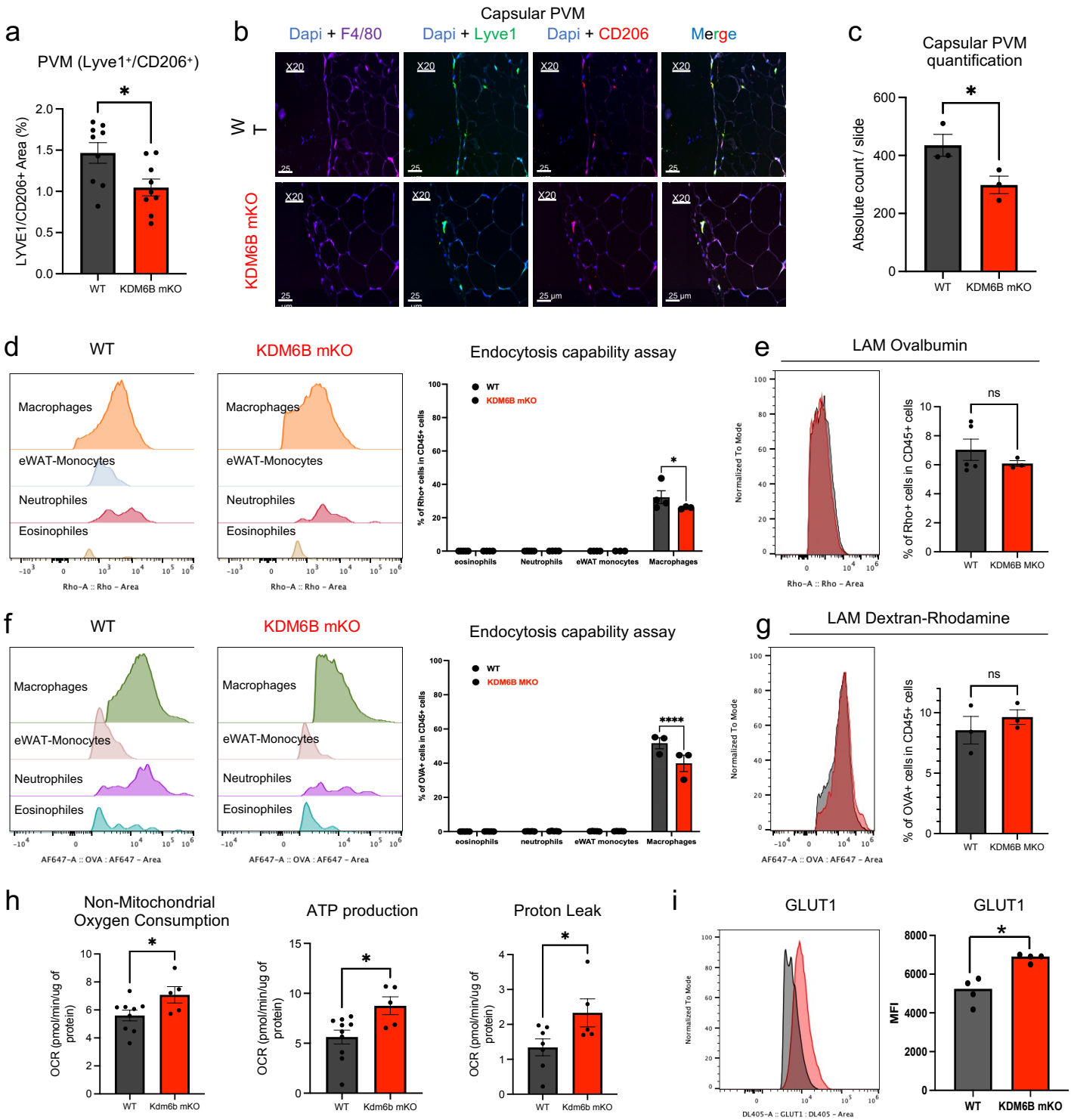

Supplementary Fig. 3 | Kdm6b loss reduces PVM abundance and metabolic activity in epididymal WAT

a, Quantification of parenchymal PVMs by immunofluorescence (IF) in WT versus mKO mice after 5-week HFD (n = 3 per genotype; 3 fields per mouse). b, Representative IF images of capsular PVMs stained for F4/80, LYVE1 and CD206; scale bar, 25 µm. c, Quantification of capsular PVMs (same cohort as a). d–g, Flow-cytometric uptake of 70 kDa dextran–rhodamine (d,e) and 45 kDa ovalbumin-AF647 (f,g) by total myeloid cells or LAMs in WT (n = 4) and mKO (n = 3). h, Seahorse extracellular-flux analysis of oxygen-consumption rate (OCR) in magnetically sorted F4/80$^+$ macrophages (WT n = 10, mKO n = 5). i, GLUT1 surface mean fluorescence intensity (MFI) in eWAT macrophages (WT n = 4, mKO n = 4). Data are mean ± s.e.m. Statistics: two-sided unpaired t-test (a,c,e,g,h,i) or two-way ANOVA with Sidak correction (d,f). ns, not significant; *P < 0.05; ****P < 0.0001.

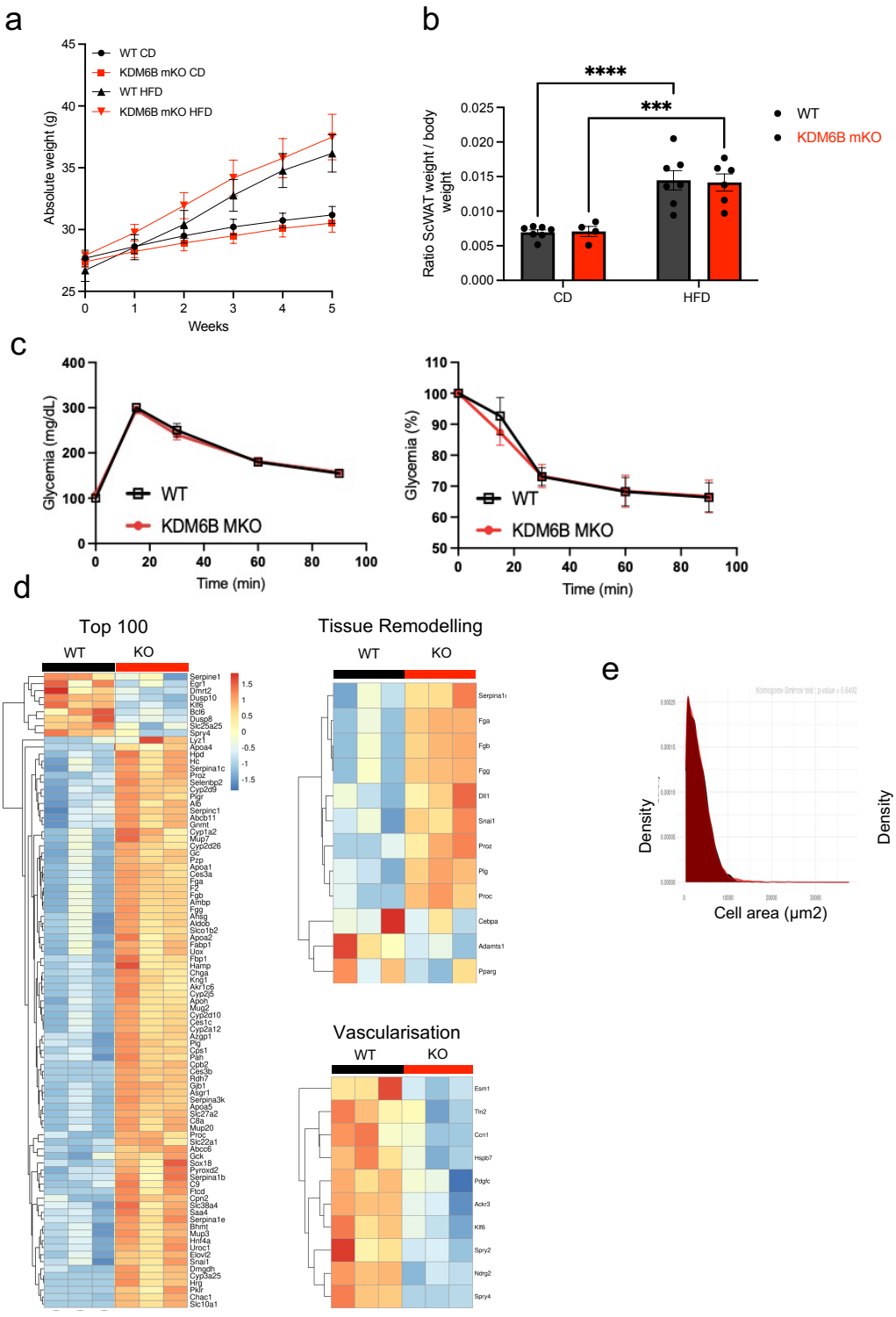

Supplementary Fig. 4 | Myeloid Kdm6b knockout alters systemic metabolism and adipose morphology

a, Absolute body mass of WT and mKO mice on chow diet (CD) or HFD for 5 weeks (CD: WT n = 10, mKO n = 9; HFD: WT n = 15, mKO n = 9). b, Relative subcutaneous WAT mass (scWAT/body-weight) in the same cohorts. c, OGTT and ITT in WT versus mKO mice on CD (n = 10 each). d, Whole-eWAT RNA-seq showing the 100 most dysregulated genes (adjusted P < 0.05) with emphasis on tissue-remodelling and vascularisation pathways (WT n = 3, mKO n = 4). e, Adipocyte-area distribution from eWAT H&E sections under CD or HFD (WT n = 3, mKO n = 3; three fields per mouse). f, IF for MAC2 to visualise crown-like structures (CLS) and their quantification after 12-week HFD (WT and mKO n = 3; three fields per mouse). Data are mean ± s.e.m. Statistics: two-way ANOVA with Tukey's post-hoc (b), DESeq2 (d), Kolmogorov–Smirnov test (e) or two-sided unpaired t-test (f). **P < 0.01; ***P < 0.001; ****P < 0.0001.

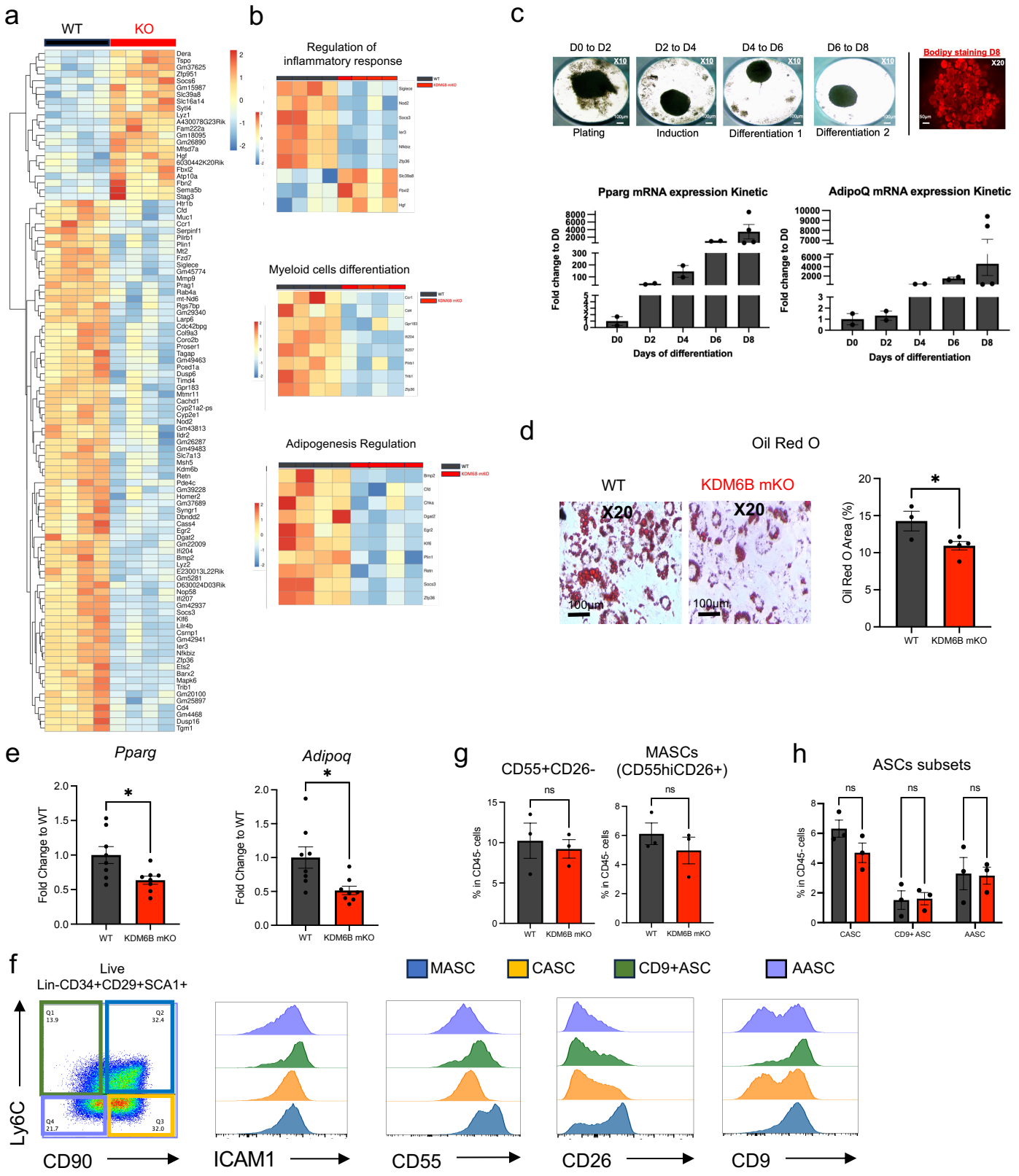

Supplementary Fig. 5 | Kdm6b deletion rewires PVM transcription and adipogenesis

a, Heat map of the 100 most deregulated genes (adjusted P < 0.05) from bulk RNA-seq of LYVE1^{+}CD206^{+} PVMs (WT and mKO n = 5). b, Sub-heat maps for GO terms “regulation of inflammatory response”, “myeloid-cell differentiation” and “adipogenesis regulation”. c, Bright-field time-course of WT eWAT organoids during HFD, Bodipy lipid staining at day 8, and time-course of Adipoq and Pparg mRNA (D0–D8; n = 2–4). d, Oil-Red-O staining of 2D adipocyte cultures from scWAT (WT n = 3, mKO n = 5) with quantification. e, Adipoq and Pparg mRNA in 2D scWAT adipocytes (WT n = 7, mKO n = 7). f, Flow-cytometry gating strategy for adipose-stem-cell (ASC) subsets. g,h, Frequency of ASC subsets, including CD55^{+}CD26^{-} and multipotent ASCs (MASC), in WT mice on CD (n = 3). Data are mean ± s.e.m. Statistics: two-sided unpaired t-test (d,e,g) or two-way ANOVA with Tukey’s post-hoc (h). ns, not significant; *P < 0.05; **P < 0.01.

a

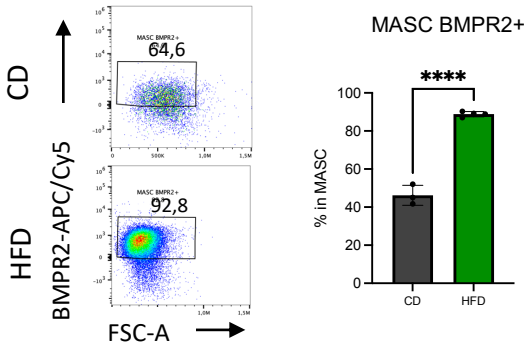

Supplementary Fig. 6 | High-fat feeding up-regulates BMPR2 on multipotent ASCs

a, BMPR2 surface MFI on MASCs from CD- and HFD-fed mice (n = 3–4). Data are mean ± s.e.m. Statistics: two-sided unpaired t-test. ns, not significant; ****P < 0.0001.

.

a

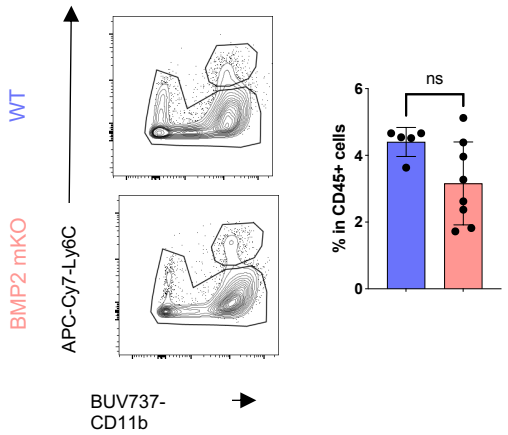

Supplementary Fig. 7 | Macrophage-specific Bmp2 deletion perturbs monocyte dynamics

a, Frequency of Ly6C^{+} monocytes in eWAT from WT (n = 5) and Bmp2 mKO (n = 8) mice after 8-week HFD, measured by flow cytometry. Data are mean ± s.e.m. Statistics: two-sided unpaired t-test. ns, not significant.

Population 1: Human scWAT

	Low KDM6B mRNA (n=12)	High KDM6B mRNA (n=12)	p
Age (y)	51 ± 11	43 ± 12	0.11
BMI (kg/m^2)	30.1 ± 3.8	30.0 ± 3.0	0.97
HbA1c (%)	6.7 ± 0.7	6.2 ± 0.8	0.14
Total cholesterol (mmol/l)	4.30 ± 0.77	5.26 ± 1.23	0.03
T2DM: N (%)	12 (100)	4 (33)	NA
KDM6B mRNA expression*	0.32 [0.15]	1.00 [0.54]	NA

Population 2: Human CD14$^+$ visWAT

	All (n=14)
Age (years)	42.37±4.14
BMI (kg/m2)	41.02±1.25
HbA1c (%)	5.92±0.31
TC (g/liter)	2.03±0.50

Population 3: Human visWAT

	All (n=6)	Obese Non-diabetic (n=3)	Obese Type-2-diabetic (n=3)
Age (years)	37,33±14.33	39±14.53	35,67±17.16
BMI (kg/m ²)	41,83±2.93	41±1.73	42,67±4.04
HbA1c (%)	5,48±0.33	5,46±0.14	5,50±0.51
TC (g/L)	1,72±0.26	1,81±0.18	1,62±0.34

Sup. Table1: Clinical profile of participants